

RSPrompter: Learning to Prompt for Remote Sensing Instance Segmentation based on Visual Foundation Model

Keyan Chen, Chenyang Liu, Hao Chen, Haotian Zhang, Wenyuan Li, Zhengxia Zou, and Zhenwei Shi*

Abstract—Leveraging vast training data (SA-1B), the foundation Segment Anything Model (SAM) proposed by Meta AI Research exhibits remarkable generalization and zero-shot capabilities. Nonetheless, as a category-agnostic instance segmentation method, SAM heavily depends on prior manual guidance involving points, boxes, and coarse-grained masks. Additionally, its performance on remote sensing image segmentation tasks has yet to be fully explored and demonstrated. In this paper, we consider designing an automated instance segmentation approach for remote sensing images based on the SAM foundation model, incorporating semantic category information. Inspired by prompt learning, we propose a method to learn the generation of appropriate prompts for SAM input. This enables SAM to produce semantically discernible segmentation results for remote sensing images, which we refer to as RSPrompter. We also suggest several ongoing derivatives for instance segmentation tasks, based on recent developments in the SAM community, and compare their performance with RSPrompter. Extensive experimental results on the WHU building, NWPU VHR-10, and SSDD datasets validate the efficacy of our proposed method. Our code is accessible at <https://kyanchen.github.io/RSPrompter>.

Index Terms—Remote sensing images, foundation model, SAM, instance segmentation, prompt learning.

I. INTRODUCTION

Instance segmentation is a crucial task in remote sensing image analysis, enabling semantic-level comprehension of each instance within remote sensing images. It provides essential information about the location (where), category (what), and shape (how) of each object [1–9]. Accurate perception and understanding of surfaces in remote sensing images significantly advance the development of remote sensing for earth observation, with applications spanning various domains including national defense, land surveying, disaster monitoring, and traffic planning [7, 10–15].

Deep learning algorithms have exhibited remarkable potential in instance segmentation for remote sensing images, demonstrating their ability to extract deep, discernible features from raw data [16–19]. Presently, the primary instance segmentation algorithms comprise two-stage R-CNN series algorithms (e.g., Mask R-CNN [20], Cascade Mask R-CNN [21], Mask Scoring R-CNN [22], HTC [23], and HQ-ISNet [1]), as well as one-stage algorithms (e.g., YOLACT [24], BlendMask [25], EmbedMask [26], Condinst [27], SOLO [28], and Mask2former [29]). However, the complexity of remote sensing image backgrounds and the diversity of scenes limit the generalization and adaptability of these algorithms. Therefore, devising instance segmentation models capable of

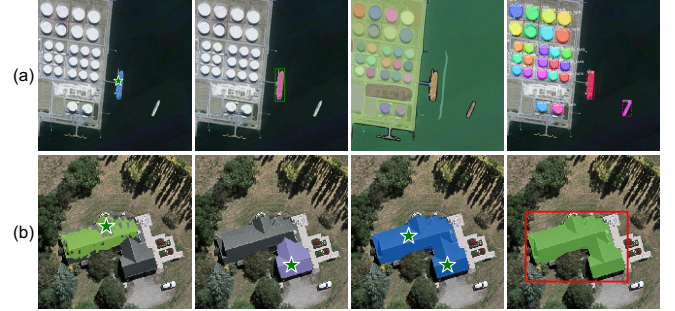


Fig. 1. (a) Depicts the instance segmentation results from point-based prompt, box-based prompt, SAM’s “everything” mode (which segments all objects in the image), and RSPrompter. SAM performs category-agnostic instance segmentation, relying on manually provided prior prompts. (b) Illustrates the segmentation results of point-based prompts from different locations, a two-point based prompt, and a box-based prompt. The type, location, and quantity of prompts heavily influence SAM’s results.

accommodating a wide range of remote sensing scenarios is crucial for interpreting remote sensing imagery.

In recent years, substantial progress has been made in foundation models, such as GPT-4 [30], Flamingo [31], and SAM [32], significantly contributing to the advancement of human society. Despite remote sensing being characterized by its big data attributes since its inception [11, 33], foundation models tailored for this field have not yet emerged. In this paper, our primary aim is not to develop a universal foundation model for remote sensing, but rather to explore the applicability of the SAM segmentation foundation model from the computer vision domain to instance segmentation in remote sensing imagery. We anticipate that such foundation models will foster the continued growth and progress of the remote sensing field.

Thanks to training on over one billion masks, SAM can segment any object in any image without additional training, showcasing its remarkable generalization capabilities when dealing with various images and objects [32]. This creates new possibilities and avenues for intelligent image analysis and understanding [34–36]. However, due to its interactive framework, SAM necessitates a prior prompt, such as a point, box, or mask, to be provided alongside the input image, and functions as a category-agnostic segmentation method, as depicted in Fig. 1 (a). Clearly, these limitations render SAM unsuitable for the fully-automatic understanding of remote-sensing images.

Moreover, we observe that the complex background interference and the lack of well-defined object edges in re-

remote sensing image scenarios present significant challenges to SAM’s segmentation capabilities. SAM struggles to execute comprehensive segmentation of remote sensing image targets, with its results being heavily reliant on the type, location, and quantity of prompts. In most cases, refined manual prompts are crucial to achieve the desired effects, as demonstrated in Fig. 1 (b). This suggests that SAM exhibits considerable limitations when applied to instance segmentation in remote-sensing images.

To enhance the remote sensing image instance segmentation of the foundation model, we propose a novel approach called RSPrompter, for learning how to generate prompts that can enhance the capabilities of the SAM framework. Just like how a person stores memories in their brain by learning a lot of knowledge or information, also known as the subconscious consciousness, we only need to learn how to recall and use these memories, without having to relearn the original knowledge. Our motivation lies in the SAM framework, where each group of prompts can obtain an instantiated mask through the mask decoder. Imagine that if we could automatically generate multiple category-related prompts, the decoder of SAM would be able to produce multiple instance-level masks with category labels. However, this process poses two main challenges: (i) Where do the category-sensitive prompts come from? (ii) What type of prompts should be selected for the input into the mask decoder?

Since SAM is a category-agnostic segmentation model, the deep feature maps of the image encoder are unlikely to contain rich semantic category information. To overcome this, we extract features from the intermediate layers of the encoder to form the input of the prompter, which generates prompts containing semantic category information. Secondly, SAM prompts include points (foreground/background points), boxes, or masks. Considering that generating point coordinates requires searching in the original SAM prompt’s manifold, which greatly limits the optimization space of the prompter, we further relax the representation of prompts and directly generate prompt embeddings, which can be understood as the embeddings of points or boxes, instead of the original coordinates. This design also avoids the obstacle of gradient flow from high-dimensional to low-dimensional and then back to high-dimensional features, *i.e.*, from high-dimension image features to point coordinates and then to positional encodings.

Additionally, we conducted a comprehensive investigation and summary of the current advancements and derivatives in the community centered on the SAM model [34, 36, 37]. These primarily encompass methods based on the SAM backbone, approaches integrating SAM with classifiers, and techniques combining SAM with detectors. Fig. 3 (a), (b), and (c) provide visual representations of these categories. A comparison with our proposed SAMPromoter, presented in this paper, is also included.

This paper presents several contributions to the field of instance segmentation in remote sensing imagery, as detailed below:

- (i) We introduce a new prompt learning technique that enhances the capabilities of the SAM model for facilitating instance segmentation in remote sensing imagery.
- (ii) We conduct an extensive evaluation of the SAM model’s performance when combined with other discriminative models for instance segmentation tasks related to remote sensing imagery.
- (iii) Our experimental findings, derived from testing multiple remote sensing instance segmentation datasets, demonstrate the effectiveness of the proposed RSPrompter.

The remainder of this paper is organized as follows: Section II provides a comprehensive review of the related works in this field. Section III delves into the detailed explanations of the extension methods based on the SAM model for instance segmentation and the proposed RSPrompter. Section IV presents both quantitative and qualitative results, including ablation studies to further support our findings. Finally, Section V concludes this paper and summarizes the key takeaways.

II. RELATED WORKS

A. Deep Learning based Instance Segmentation

The objective of instance segmentation is to identify the location of each target instance within an image and provide a corresponding semantic mask, making this task more challenging than object detection and semantic segmentation [18, 38]. Current deep learning-based instance segmentation approaches can be broadly categorized into two-stage and single-stage methods. The former primarily builds on the Mask R-CNN [20] series, which evolved from the two-stage Faster R-CNN [39] object detector by incorporating a parallel mask prediction branch. As research advances, an increasing number of researchers are refining this framework to achieve improved performance. PANet [16] streamlines the information path between features by introducing a bottom-up path based on FPN [40]. In HTC [23], a multi-task, multi-stage hybrid cascade structure is proposed, and the spatial context is enhanced by integrating the segmentation branch, resulting in significant performance improvements over Mask R-CNN and Cascade Mask R-CNN [21]. The Mask Scoring R-CNN [22] incorporates a mask IoU branch within the Mask R-CNN framework to assess segmentation quality. The HQ-ISNet [1] introduces an instance segmentation method for remote sensing imagery based on Cascade Mask R-CNN, which fully leverages multi-level feature maps and preserves the detailed information contained within high-resolution images.

Though two-stage methods can yield refined segmentation results, achieving the desired latency in terms of segmentation speed remains challenging. With the growing popularity of single-stage object detectors, numerous researchers have endeavored to adapt single-stage object detectors for instance segmentation tasks. YOLACT [24], for example, approaches the instance segmentation task by generating a set of prototype masks and predicting mask coefficients for each instance. CondInst [27] offers a fresh perspective on the instance segmentation problem by employing a dynamic masking head. This novel approach has outperformed existing methods like Mask R-CNN in terms of instance segmentation performance. SOLO [28] formulates the instance segmentation problem as predicting semantic categories and generating instance masks for each pixel in the feature map. With the widespread adoption of Transformers [41], DETR [42] has emerged as a fully

end-to-end object detector. Drawing inspiration from the task modeling and training procedures used in DETR, Maskformer [43] treats segmentation tasks as mask classification problems, but it suffers from slow convergence speed. Mask2former [29] introduces masked attention to confine cross-attention to the foreground region, significantly improving network training speed.

Instance segmentation and object detection tasks are mutually reinforcing, and their development has reached a plateau at the technical level. Presently, research on foundational segmentation and detection models has become a popular area of focus [32, 44–48]. In this paper, we investigate the performance of the SAM foundation model when applied to instance segmentation tasks in remote sensing imagery.

B. Foundation Model

In recent years, foundation models have ignited a groundbreaking wave in the field of artificial intelligence. Owing to their training on vast amounts of data, these models demonstrate remarkable zero-shot generalization capabilities across various scenarios [32, 49, 50]. The concept of pre-training large models initially emerged and evolved within the realm of natural language processing (NLP), marked by the development of foundational language models such as BERT [51], T5 [52], and GPT [30, 53–55]. In the past year, well-known models like Chat-GPT [56] and GPT-4 [30] have further revolutionized the advancement of artificial intelligence, even contributing to the progress of human civilization and making significant impacts across various industries.

Inspired by the success of foundational models in NLP, researchers have sought to explore their potential within the realm of computer vision. In terms of architecture, they have begun adopting the Transformer for the visual domain, investigating large models such as ViT-G [57], ViT-22B [58], and Swin Transformer v2 [59]. Drawing inspiration from BERT’s training regimen, MAE [60] was the first to propose a Transformer-based visual masking training strategy, which yielded significant results across numerous downstream tasks. A vast amount of freely available image-text paired data can be found online. CLIP [49] and ALIGN [50] employ contrastive learning to align visual and textual spaces within noisy image-text pairs, extracting valuable semantic knowledge and demonstrating robust zero-shot transfer capabilities across downstream tasks [61, 62]. Other large models like Flamingo [31] learn representations from arbitrarily interleaved text and image corpora on the web.

While most of these models aim to extract available knowledge from free data, the recent SAM model [32] goes a step further by constructing a data engine in which the model is co-developed alongside model-in-the-loop dataset annotation. SAM uniquely employs an extensive amount of masks (11 million images, comprising over 1 billion masks), exhibiting strong generalization capabilities. However, the original intention was to develop a task-agnostic (*i.e.*, unable to provide labels for segmented objects) segmentation model requiring prompts (*i.e.*, input of prior points, bounding boxes, or masks). As such, it cannot achieve end-to-end automated segmentation

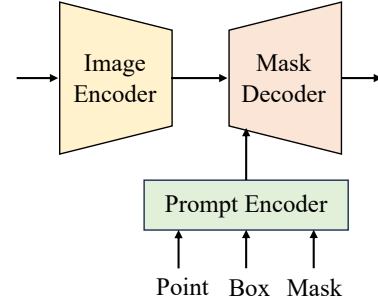


Fig. 2. A schematic representation of SAM is depicted, which comprises an image encoder, a prompt encoder, and a mask decoder. SAM produces corresponding object masks based on the input prompts provided.

perception. In this paper, we do not delve into the design and training of a foundational remote sensing instance segmentation model. Instead, we explore the applicability of SAM’s powerful general segmentation capabilities to remote-sensing images, aiming to inspire readers and fellow researchers. Furthermore, the proposed learn-to-prompt method can be applied to other foundation visual models beyond SAM for task-specific or domain-specific downstream tasks.

C. Prompt Learning

For many years, machine learning tasks primarily focused on fully supervised learning, wherein task-specific models were trained solely on labeled examples of the target task [63, 64]. Over time, the learning of these models has undergone a significant transformation, shifting from fully supervised learning to a “pre-training and fine-tuning” paradigm for downstream tasks. This allows models to utilize the general features obtained during pre-training [65–68]. As the field has evolved, the “pre-training and fine-tuning” approach is being increasingly replaced with a “pre-training and prompting” paradigm [61, 62, 69–72]. In this new paradigm, researchers no longer adapt the model exclusively to downstream tasks but rather redesign the input using prompts to reconstruct downstream tasks to align with the original pre-training task [49, 51, 54].

Prompt learning can help reduce semantic differences (bridging the gap between pre-training and fine-tuning) and prevent overfitting of the head. Since the introduction of GPT-3 [55], prompt learning has progressed from traditional discrete [71] and continuous prompt construction [61, 72] to large-scale model-oriented in-context learning [31], instruction-tuning [73–75], and chain-of-thought approaches [76–78]. Current methods for constructing prompts mainly involve manual templates, heuristic-based templates, generation, word embedding fine-tuning, and pseudo tokens [71, 79]. In this paper, we propose a prompt generator that generates SAM-compatible prompt inputs. This prompt generator is category-related and produces semantic instance segmentation results.

III. METHODOLOGY

In this section, we will present our proposed RSPrompter, a learning-to-prompt method based on the SAM framework for

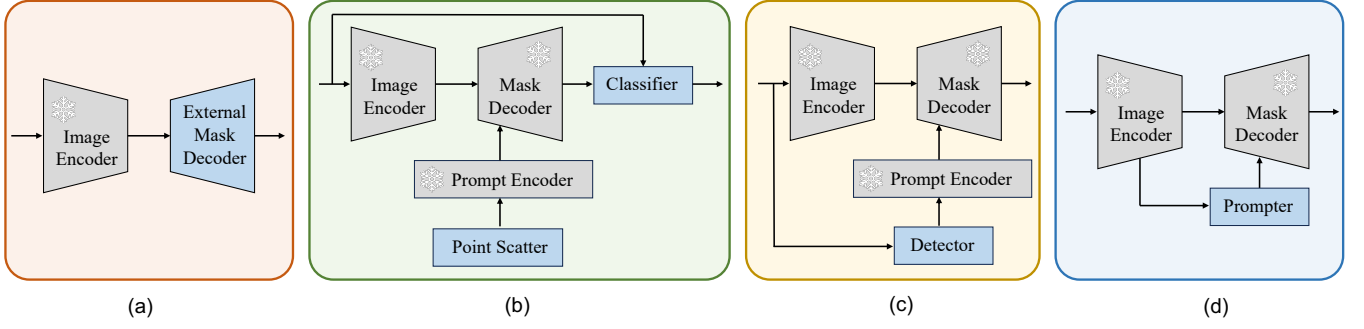


Fig. 3. From left to right, the figure illustrates SAM-seg, SAM-cls, SAM-det, and RSPrompter as alternative solutions for applying SAM to remote sensing image instance segmentation tasks. (a) An instance segmentation head is added after SAM’s image encoder. (b) SAM’s “everything” mode generates masks for all objects in an image, which are subsequently classified into specific categories by a classifier. (c) Object bounding boxes are first produced by an object detector and then used as prior prompts input to SAM to obtain the corresponding masks. (d) The proposed RSPrompter in this paper creates category-relevant prompt embeddings for instant segmentation masks. The snowflake symbol in the figure signifies that the model parameters in this part are kept frozen.

remote sensing image instance segmentation. We will cover the following aspects: revisiting SAM, incorporating simple extensions to tailor SAM for the instance segmentation task, and introducing both anchor-based and query-based RSPrompter along with their respective loss functions.

A. A Revisit of SAM

SAM is an interactive segmentation framework that generates segmentation results based on given prompts, such as foreground/background points, bounding boxes, or masks. It comprises three main components: an image encoder (Φ_{i-enc}), a prompt encoder (Φ_{p-enc}), and a mask decoder (Φ_{m-dec}). SAM employs a pre-trained Masked AutoEncoder (MAE) [60] based on Vision Transformer (ViT) [80] to process images into intermediate features, and encodes the prior prompts as embedding tokens. Subsequently, the cross-attention mechanism within the mask decoder facilitates the interaction between image features and prompt embeddings, ultimately resulting in a mask output. This process can be illustrated in Fig. 2 and expressed as:

$$\begin{aligned} F_{img} &= \Phi_{i-enc}(\mathcal{I}) \\ T_{prompt} &= \Phi_{p-enc}(\{p\}) \\ \mathcal{M} &= \Phi_{m-dec}(F_{img} + F_{c-mask}, [T_{out}, T_{prompt}]) \end{aligned} \quad (1)$$

where $\mathcal{I} \in \mathbb{R}^{H \times W \times 3}$ represents the original image, $F_{img} \in \mathbb{R}^{h \times w \times c}$ denotes the intermediate image features, $\{p\}$ encompasses the sparse prompts including foreground/background points and bounding boxes, and $T_{prompt} \in \mathbb{R}^{k \times c}$ signifies the sparse prompt tokens encoded by Φ_{p-enc} . Additionally, $F_{c-mask} \in \mathbb{R}^{h \times w \times c}$ refers to the representation from the coarse mask, which is an optional input for SAM, while $T_{out} \in \mathbb{R}^{5 \times c}$ consists of the pre-inserted learnable tokens representing four different masks and their corresponding IoU predictions. Finally, \mathcal{M} corresponds to the predicted masks. In this task, diverse outputs are not required, so we directly select the first mask as the final prediction.

B. Extensions on SAM for Instance Segmentation

We have conducted a survey within the SAM community and, in addition to the RSPrompter proposed in this paper, have also introduced three other SAM-based instance segmentation methods for comparison, as shown in Fig. 3 (a), (b), and (c), to assess their effectiveness in remote sensing image instance segmentation tasks and inspire future research. These methods include: an external instance segmentation head, classifying mask categories, and using detected object boxes, which correspond to Fig. 3 (a), (b), and (c), respectively. In the following sections, we will refer to these methods as SAM-seg, SAM-cls, and SAM-det, respectively.

1) *SAM-seg*: In SAM-seg, we make use of the knowledge present in SAM’s image encoder while maintaining the cumbersome encoder frozen. We extract intermediate-layer features from the encoder, conduct feature fusion using convolutional blocks, and then perform instance segmentation tasks with existing instance segmentation heads, such as Mask R-CNN [20] and Mask2Former [29]. This process can be described using the following equations:

$$\begin{aligned} \{F_i\} &= \Phi_{i-enc}(\mathcal{I}) \\ F_i &= \text{DownConv}(F_i) \\ F &= \text{FusionConv}([F_1, \dots, F_k]) \\ \mathcal{M} &= \Phi_{ext-dec}(F) \end{aligned} \quad (2)$$

where $\{F_i\} \in \mathbb{R}^{k \times h \times w \times c}$, $i \in \{1, \dots, k\}$ represents multi-layer semantic feature maps from the ViT backbone. DownConv refers to a 1×1 convolution operation that reduces channel dimensions, while $[\cdot]$ denotes concatenation alongside the channel axis. FusionConv is a stack of three convolutional layers with 3×3 kernels and a ReLU activation following each layer. $\Phi_{ext-dec}$ represents the externally inherited instance segmentation head, such as Mask R-CNN [20] and Mask2Former [29]. It is important to note that the image encoder remains frozen, and this training method does not utilize multi-scale loss supervision, as in Mask R-CNN and Mask2Former.

2) *SAM-cls*: In SAM-cls, we first utilize the “everything” mode of SAM to segment all potential instance targets within the image. Internally, this is achieved by uniformly scattering

points throughout the image and treating each point as a prompt input for an instance. After obtaining the masks of all instances in the image, we can assign labels to each mask using a classifier. This process can be described as follows:

$$\begin{aligned}
 F_{\text{img}} &= \Phi_{\text{i-enc}}(\mathcal{I}) \\
 T_{(i,j)} &= \Phi_{\text{p-enc}}((x_i, y_j)) \\
 \mathcal{M}_{(i,j)} &= \Phi_{\text{m-dec}}(F_{\text{img}}, [T_{\text{out}}, T_{(i,j)}]) \\
 c_{(i,j)} &= \Phi_{\text{ext-clc}}(\mathcal{I}, \mathcal{M}_{(i,j)})
 \end{aligned} \tag{3}$$

where (x_i, y_j) represents the point prompt. For every image, we consider 32×32 points to generate category-agnostic instance masks. $\Phi_{\text{ext-clc}}$ denotes the external mask classifier, and $c_{(i,j)}$ refers to the labeled category. For convenience, we directly use the lightweight ResNet18 [68] to label the masks. It performs classification by processing the original image patch cropped by the mask. When cropping the image, we first enlarge the crop box by 2 times and then blur non-mask areas to enhance the discriminative capability. To achieve better performance, the mask's classification representation could be extracted from the image encoder's intermediate features, but we chose not to follow that approach for the sake of simplicity in our paper. Alternatively, a pre-trained CLIP model can be leveraged, allowing SAM-clc to operate in a zero-shot regime without additional training.

3) *SAM-det*: The SAM-det method is more straightforward to implement and has gained widespread adoption in the community. First, we train an object detector to identify the desired targets in the image, and then input the detected bounding boxes as prompts into SAM. The entire process can be described as follows:

$$\begin{aligned}
 b_i &= \Phi_{\text{ext-det}}(\mathcal{I}) \\
 F_{\text{img}} &= \Phi_{\text{i-enc}}(\mathcal{I}) \\
 T_i &= \Phi_{\text{p-enc}}(b_i) \\
 \mathcal{M}_i &= \Phi_{\text{m-dec}}(F_{\text{img}}, [T_{\text{out}}, T_i])
 \end{aligned} \tag{4}$$

where b_i represents bounding boxes detected by the external pre-trained object detector, $\Phi_{\text{ext-det}}$. Here, we employ Faster R-CNN [39] as the detector.

C. RSPrompter

1) *Overview*: The proposed RSPrompter's structure is illustrated in Fig. 3 (d). Suppose we have a training dataset, i.e., $\mathcal{D}_{\text{train}} = \{(\mathcal{I}_1, y_1), \dots, (\mathcal{I}_N, y_N)\}$, where $\mathcal{I}_i \in \mathbb{R}^{H \times W \times 3}$ denotes an image, and $y_i = \{b_i, c_i, m_i\}$ represents its corresponding ground-truth annotations, including the coordinates of n object bounding boxes ($b_i \in \mathbb{R}^{n_i \times 4}$), their associated semantic categories ($c_i \in \mathbb{R}^{n_i \times \mathcal{C}}$), and binary masks ($m_i \in \mathbb{R}^{n_i \times H \times W}$). Our objective is to train a prompter for SAM that can process any image from a test set ($\mathcal{I}_k \sim \mathcal{D}_{\text{test}}$), simultaneously localizing the objects and inferring their semantic

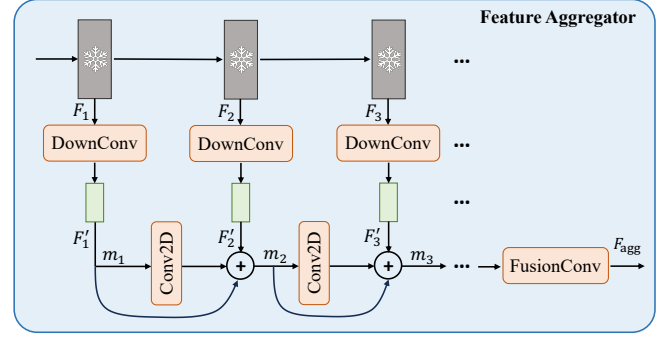


Fig. 4. The figure illustrates the proposed lightweight feature aggregator, which extracts semantic information from the large ViT backbone and performs a lightweight fusion process.

categories and instance masks, which can be expressed as follows:

$$\begin{aligned}
 F_{\text{img}}, \{F_i\} &= \Phi_{\text{i-enc}}(\mathcal{I}_k) \\
 F_{\text{agg}} &= \Phi_{\text{aggregator}}(\{F_i\}) \\
 \{T_j, c_j\} &= \Phi_{\text{prompter}}(F_{\text{agg}}) \\
 \mathcal{M}_j &= \Phi_{\text{m-dec}}(F_{\text{img}}, [T_{\text{out}}, T_j])
 \end{aligned} \tag{5}$$

where the image is processed by the frozen SAM image encoder to generate $F_{\text{img}} \in \mathbb{R}^{h \times w \times c}$ and multiple intermediate feature maps $\{F_i\} \in \mathbb{R}^{k \times h \times w \times c}$. F_{img} is used by the SAM decoder to obtain prompt-guided masks, while F_i is progressively processed by an efficient feature aggregator ($\Phi_{\text{aggregator}}$) and a prompt generator (Φ_{prompter}) to acquire multiple groups of prompts ($T_j \in \mathbb{R}^{k_p \times c}, j \in \{1, \dots, N_p\}$) and corresponding semantic categories ($c_j \in \mathbb{R}^{\mathcal{C}}, j \in \{1, \dots, N_p\}$). k_p defines the number of prompt embeddings needed for each mask generation. We will employ two distinct structures to design the prompt generator, namely anchor-based and query-based.

It is important to note that T_j only contains foreground target instance prompts, with the semantic category given by c_j . A single T_j is a combination of multiple prompts, i.e., representing an instance mask with multiple point embeddings or a bounding box. For simplicity, we will omit the superscript k when describing the proposed model.

2) *Feature Aggregator*: SAM is a category-agnostic segmentation model based on prompts. To obtain semantically relevant and discriminative features without increasing the computational complexity of the prompter, we introduce a lightweight feature aggregation module. This module learns to represent semantic features from various intermediate feature layers of the SAM ViT backbone, as depicted in Fig. 4. The module can be described recursively as follows:

$$\begin{aligned}
 F'_i &= \Phi_{\text{DownConv}}(F_i) \\
 m_1 &= F'_1 \\
 m_i &= m_{i-1} + \Phi_{\text{Conv2D}}(m_{i-1}) + F'_i \\
 F_{\text{agg}} &= \Phi_{\text{FusionConv}}(m_k)
 \end{aligned} \tag{6}$$

where $F_i \in \mathbb{R}^{h \times w \times c}$ and $F'_i \in \mathbb{R}^{\frac{h}{2} \times \frac{w}{2} \times \frac{c}{16}}$ indicate the SAM backbone's features and down-sampled features generated by

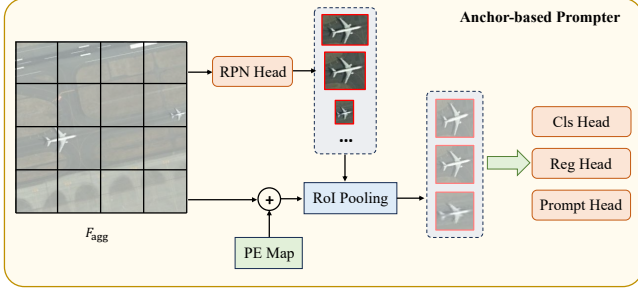


Fig. 5. The figure presents a diagram of the proposed anchor-based prompter.

Φ_{DownConv} . This process first employs a 1×1 Convolution-ReLU block to reduce the channels from c to $\frac{c}{16}$, followed by a 3×3 Convolution-ReLU block with a stride of 2 to decrease the spatial dimensions. Since we believe that only coarse information about the target location is necessary, we boldly further reduce the spatial dimension size to minimize computational overhead. Φ_{Conv2D} denotes a 3×3 Convolution-ReLU block, while $\Phi_{\text{FusionConv}}$ represents the final fusion convolutional layers comprising two 3×3 convolution layers and one 1×1 convolution layer to restore the original channel dimensions of SAM’s mask decoder.

3) *Anchor-based Prompter*: Upon obtaining the fused semantic features, we can employ the prompter to generate prompt embeddings for the SAM mask decoder. In this section, we introduce the anchor-based approach for generating prompt embeddings.

Architecture: First, we generate candidate object boxes using the anchor-based Region Proposal Network (RPN). Next, we obtain the individual object’s visual feature representation from the positional encoding feature map via RoI Pooling [20], according to the proposal. From the visual feature, we derive three perception heads: the semantic head, the localization head, and the prompt head. The semantic head determines a specific object category, while the localization head establishes the matching criterion between the generated prompt representation and the target instance mask, *i.e.*, greedy matching based on localization (Intersection over Union, or IoU). The prompt head generates the prompt embedding required for the SAM mask decoder. The entire process is illustrated in Fig. 5 and can be represented by the following equation:

$$\begin{aligned}
 \{b_j\} &= \Phi_{\text{rpn}}(F_{\text{agg}}) \\
 v_j &= \Phi_{\text{roi-p}}(F_{\text{agg}} + \text{PE}, b_j) \\
 c_j &= \Phi_{\text{cls}}(v_j) \\
 b_j &= \Phi_{\text{reg}}(v_j) \\
 T_j &= \Phi_{\text{prompt}}(v_j) \\
 T_j &= T_j + \sin T_j
 \end{aligned} \tag{7}$$

where Φ_{rpn} represents a lightweight RPN. Since the $\Phi_{\text{roi-p}}$ operations may cause the subsequent prompt generation to lose positional information relative to the entire image, we incorporate positional encoding (PE) into the original fused features (F_{agg}). The functions Φ_{cls} , Φ_{reg} , and Φ_{prompt} correspond to the

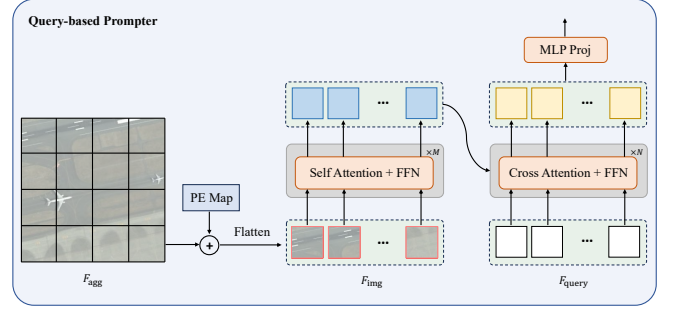


Fig. 6. An illustration of the proposed query-based prompter.

semantic head, the localization head, and the prompt head, respectively.

To align the embeddings from SAM’s prompt encoder with the generated prompt embeddings, we use sine functions to directly generate high-frequency information rather than predicting it through the network. This is because neural networks have difficulty predicting high-frequency information. The effectiveness of this design has been confirmed through subsequent experiments.

Loss Function: In the anchor-based prompter, the primary framework adheres to the structure of Faster R-CNN [39]. The various losses incorporated within this model include binary classification loss and localization loss for the RPN network, classification loss for the semantic head, regression loss for the localization head, and segmentation loss for the frozen SAM mask decoder. Consequently, the overall loss can be expressed as follows:

$$\mathcal{L}_{\text{anchor}} = \frac{1}{M} \sum_i \mathcal{L}_{\text{rpn}}^i + \frac{1}{N} \sum_j (\mathcal{L}_{\text{cls}}^j + \mathbb{1}^j (\mathcal{L}_{\text{reg}}^j + \mathcal{L}_{\text{seg}}^j)) \tag{8}$$

where \mathcal{L}_{cls} represents the Cross-Entropy loss calculated between the predicted category and the target, while \mathcal{L}_{reg} denotes the SmoothL1 loss computed based on the predicted coordinate offsets and the target offsets between the ground truth and the prior box. Furthermore, \mathcal{L}_{seg} indicates the binary cross-entropy loss between the SAM-decoded mask and the target instance mask label, where the matching criteria are determined by the IoU of the boxes. The indicator function $\mathbb{1}$ is employed to confirm a positive match. Lastly, \mathcal{L}_{rpn} signifies the region proposal loss.

4) *Query-based Prompter*: The anchor-based prompter procedure is relatively intricate, involving the utilization of box information for mask matching and supervised training. To streamline this process, we propose a query-based prompter that employs optimal transport as its foundation.

Architecture: The query-based prompter primarily consists of a lightweight Transformer encoder and decoder internally. The encoder is employed to extract high-level semantic features from the image, while the decoder is utilized to transform the preset learnable query into the requisite prompt embedding for SAM via cross-attention interaction with image features. The

entire process is depicted in Fig. 6, as follows:

$$\begin{aligned}
F'_{\text{img}} &= \Phi_{\text{T-enc}}(F_{\text{agg}} + \text{PE}) \\
F_{\text{query}} &= \Phi_{\text{T-dec}}(F'_{\text{img}}, F_{\text{query}}) \\
C &= \Phi_{\text{mlp-cls}}(F_{\text{query}}) \\
T &= \Phi_{\text{mlp-prompt}}(F_{\text{query}}) \\
T &= T + \sin T
\end{aligned} \tag{9}$$

where $\text{PE} \in \mathbb{R}^{h \times w \times c}$ refers to the positional encoding, while $F_{\text{query}} \in \mathbb{R}^{N_p \times c}$ represents the learnable tokens, which are initialized as zero. $\Phi_{\text{mlp-cls}}$ constitutes an MLP layer employed to obtain class predictions ($C \in \mathbb{R}^{N_p \times c}$). Meanwhile, $\Phi_{\text{mlp-prompt}}$ comprises a two-layer MLP designed to acquire the projected prompt embeddings ($T \in \mathbb{R}^{N_p \times k_p \times c}$). N_p denotes the number of prompt groups, *i.e.*, the number of instances. k_p defines the number of embeddings per prompt, *i.e.*, the number of prompts necessary to represent an instance target. Furthermore, $\Phi_{\text{T-enc}}$ and $\Phi_{\text{T-dec}}$ symbolize the Transformer encoder and decoder, respectively.

Loss Function: The training process for the query-based prompter primarily involves two key steps: (i) matching N_p masks, decoded by the SAM mask decoder, to K ground-truth instance masks (typically, $N_p > K$); (ii) subsequently conducting supervised training using the matched labels. While executing optimal transport matching, we define the matching cost, taking into account the predicted category and mask, as detailed below:

$$\begin{aligned}
\Omega &= \arg \min_{\omega} \sum_i^N \mathcal{L}_{\text{match}}(\hat{y}_i, y_{\omega(i)}) \\
\mathcal{L}_{\text{match}} &= \mathcal{L}_{\text{cls}} + \mathcal{L}_{\text{seg-ce}} + \mathcal{L}_{\text{seg-dice}}
\end{aligned} \tag{10}$$

where ω represents the assignment relationship, while \hat{y}_i and y_i correspond to the prediction and the label, respectively. We employ the Hungarian algorithm [81] to identify the optimal assignment between the N_p predictions and K targets. The matching cost considers the similarity between predictions and ground-truth annotations. Specifically, it incorporates the class classification matching cost (\mathcal{L}_{cls}), mask cross-entropy cost ($\mathcal{L}_{\text{seg-ce}}$), and mask dice cost ($\mathcal{L}_{\text{seg-dice}}$).

Once each predicted instance is paired with its corresponding ground truth, we can readily apply the supervision terms. These primarily comprise multi-class classification and binary mask classification, as described below:

$$\mathcal{L}_{\text{query}} = \frac{1}{N_p} \sum_i^{N_p} (\mathcal{L}_{\text{cls}}^i + \mathbb{1}^i \mathcal{L}_{\text{seg}}^i) \tag{11}$$

where \mathcal{L}_{cls} denotes the cross-entropy loss computed between the predicted category and the target, while \mathcal{L}_{seg} signifies the binary cross-entropy loss between the SAM decoded mask and the matched ground-truth instance mask. Additionally, $\mathbb{1}$ represents the indicator function.

IV. EXPERIMENTAL RESULTS AND ANALYSES

A. Experimental Dataset and Settings

In this paper, we employ three public remote sensing instance segmentation datasets – the WHU building extraction dataset [82], NWPU VHR-10 dataset [2, 83], and SSDD dataset [1, 84] – to validate the efficacy of the proposed method. These datasets have been extensively utilized in the realm of remote sensing instance segmentation [1, 2, 4, 85].

WHU [82]: We utilize the aerial imagery subset in the WHU building extraction dataset. This subset comprises 8188 non-overlapping RGB images of size 512×512 pixels. The images are captured above Christchurch, New Zealand, with a spatial resolution ranging from 0.0075m to 0.3m. We adhere to the official settings, designating 4736 images for the training set, 1036 for the validation set, and 2416 for the test set. To obtain instance annotations, we employ the connected component analysis method from the OpenCV library, enabling the conversion of semantic segmentation into an instance segmentation format.

NWPU [83]: The NWPU VHR-10 dataset comprises a remote sensing image object detection dataset consisting of ten classes: airplane, ship, storage tank, baseball diamond, tennis court, basketball court, ground track field, harbor, bridge, and vehicle. It encompasses 715 optical remote sensing images from Google Earth with a spatial resolution of 0.5-2m and 85 pan-sharpened color infrared images from the Vaihingen dataset with a spatial resolution of 0.08m. In our study, we allocate 80% of the data for training and 20% for testing. We employ the instance annotations provided by [2] for training and evaluation purposes.

SSDD [84]: The SAR Ship Detection Dataset (SSDD) encompasses 1160 SAR images with a resolution range from 1 to 15 meters, and 2540 ship instances. We randomly assign 80% of the images for training and 20% for testing. The instance masks are annotated by [1].

B. Evaluation Protocol and Metrics

To evaluate the performance of the proposed method, we employ the widely adopted COCO [86] mean average precision (mAP) metric. This metric is commonly utilized to objectively assess the effectiveness of object detection or instance segmentation methods [9, 39, 61]. A prediction is considered a true positive when the predicted box or mask of an instance has an intersection over union (IoU) with its corresponding ground truth greater than a threshold T and when its predicted category matches. In this paper, we use $\text{AP}_{\text{box}}^{50}$, $\text{AP}_{\text{box}}^{75}$, $\text{AP}_{\text{mask}}^{50}$, and $\text{AP}_{\text{mask}}^{75}$ for evaluation. The term AP refers to metrics averaged across all 10 IoU thresholds (0.50 : 0.05 : 0.95) and all categories. A larger AP value indicates more accurate predicted instance masks and, consequently, better instance segmentation performance. AP^{50} represents the calculation under the IoU threshold of 0.50, while AP^{75} embodies a stricter metric that corresponds to the calculation under the IoU threshold of 0.75. As such, AP^{75} outperforms AP^{50} in the evaluation of mask accuracy,

TABLE I

THE TABLE PRESENTS A COMPARISON BETWEEN THE PROPOSED METHOD AND OTHER STATE-OF-THE-ART METHODS ON THE WHU DATASET. IT DISPLAYS AP(%) VALUES FOR BOXES AND MASKS AT VARIOUS IOU THRESHOLDS.

Method	AP _{box}	AP _{box} ⁵⁰	AP _{box} ⁷⁵	AP _{mask}	AP _{mask} ⁵⁰	AP _{mask} ⁷⁵
Mask R-CNN [20]	56.11	80.16	63.34	60.75	84.15	71.43
MS R-CNN [22]	54.91	79.94	62.76	53.44	80.08	62.30
HTC [23]	58.55	81.52	67.25	56.66	81.97	66.59
InstaBoost [87]	54.90	80.98	62.80	57.77	82.38	68.10
SOLO [28]	50.96	74.86	57.20	60.10	81.95	70.35
PointRend [88]	50.19	76.57	57.34	51.90	77.45	60.75
SOLOv2 [89]	45.92	74.33	49.74	49.10	78.37	56.21
SCNet [90]	58.42	81.04	67.02	57.51	81.46	67.26
CondInst [27]	53.89	81.31	60.25	51.99	81.70	59.59
BoxInst [91]	52.35	80.72	58.35	39.04	77.67	36.51
Mask2Former [29]	60.40	82.68	68.50	62.77	85.65	72.65
CATNet [5]	59.57	84.27	67.50	61.13	85.55	70.72
HQ-ISNet [1]	61.20	84.95	68.90	62.30	86.70	71.53
SAM-seg (Mask2Former)	67.84	87.35	76.74	66.66	88.19	77.09
SAM-seg (Mask R-CNN)	67.15	88.11	76.50	64.86	88.00	73.75
SAM-cls	39.93	65.35	40.64	38.26	59.18	42.53
SAM-det	66.54	89.11	76.87	61.87	88.49	71.34
RSPrompter-query	70.36	89.24	79.08	69.21	90.15	79.88
RSPrompter-anchor	68.06	87.29	76.60	66.89	88.19	77.14

with a greater AP⁷⁵ value signifying more accurate instance masks.

C. Implementation Details

The proposed method concentrates on learning to prompt remote sensing image instance segmentation using the SAM foundation model. In our experiments, we employ the ViT-Huge backbone of SAM, unless otherwise indicated.

1) *Architecture Details*: The SAM framework generates various segmentations for a single prompt; however, our method anticipates only one instance mask for each learned prompt. Consequently, we select the first mask as the final output. For each group of prompts, we set the number of prompts to 4, *i.e.*, $k_p = 4$. In the feature aggregator, to reduce computation costs, we use input features from every 3 layers after the first 8 layers of the backbone, rather than from every layer. For the anchor-based prompter, the RPN network originates from Faster R-CNN [39], and other hyperparameters in the training remain consistent. For the query-based prompter, we employ a 1-layer transformer encoder and a 4-layer transformer decoder, implementing multi-scale training for category prediction from the outputs of the decoder at 4 different levels. However, we do not apply multi-scale training to instance mask prediction in order to maintain efficiency. We determine the number of learnable tokens based on the distribution of target instances in each image, *i.e.*, $N_p = 90, 60, 30$ for the WHU, NWPU, and SSDD datasets, respectively.

2) *Training Details*: During the training phase, we adhere to the image size of 1024×1024 , in line with SAM's original input. Concurrently, we utilize horizontal flipping to augment

the training samples, without implementing any additional enhancements. Other comparative methods also follow the same settings unless specified otherwise. We only train the parameters of the prompter component while maintaining the parameters of other parts of the network as frozen. During the testing phase, we predict up to 100 instance masks per image for evaluation purposes.

For optimization, we employ the AdamW optimizer with an initial learning rate of $2e - 4$ to train our model. We set the mini-batch size to 24. The total training epochs are 700/1000 for the WHU dataset and 1500/2500 for both the NWPU and SSDD datasets (RSPrompter-anchor/RSPrompter-query). We implement a Cosine Annealing scheduler [92] to decay the learning rate. Our proposed method is developed using PyTorch, and we train all the extra-designed modules from scratch.

D. Comparison with the State-of-the-Art

In this section, we compare our proposed method with several other state-of-the-art instance segmentation methods. These include multi-stage approaches such as Mask R-CNN [20], Mask Scoring (MS) R-CNN [22], HTC [23], InstaBoost [87], PointRend [88], SCNet [90], CATNet [5], and HQ-ISNet [1], as well as single-stage methods like SOLO [28], SOLOv2 [89], CondInst [27], BoxInst [91], and Mask2Former [29]. Among these, SOLOv2 [89], CondInst [27], BoxInst [91], and Mask2Former [29] are filter-based methods, while CATNet [5] and HQ-ISNet [1] are Mask R-CNN-based remote sensing instance segmentation methods. For extending instance segmentation methods on SAM, we carry out SAM-seg (Mask R-CNN) and SAM-seg (Mask2Former) for SAM-seg with

TABLE II

THE TABLE ILLUSTRATES A COMPARISON BETWEEN THE PROPOSED METHOD AND OTHER STATE-OF-THE-ART METHODS ON THE NWPU DATASET. IT EXHIBITS AP(%) VALUES FOR BOXES AND MASKS AT DISTINCT IOU THRESHOLDS.

Method	AP _{box}	AP _{box} ⁵⁰	AP _{box} ⁷⁵	AP _{mask}	AP _{mask} ⁵⁰	AP _{mask} ⁷⁵
Mask R-CNN [20]	52.64	80.37	58.52	54.22	79.40	59.35
Mask Scoring R-CNN [22]	52.95	83.80	58.20	57.92	82.17	66.00
HTC [23]	58.78	82.98	69.10	58.20	83.27	65.32
InstaBoost [87]	43.45	74.93	44.93	48.77	75.52	49.01
SOLO [28]	45.91	70.66	50.06	45.34	71.46	46.30
PointRend [88]	36.90	70.76	33.99	44.19	71.45	43.77
SOLO v2 [89]	33.90	63.67	32.52	35.03	59.32	33.72
SCNet [90]	48.62	78.03	54.01	50.51	78.86	51.21
CondInst [27]	34.50	66.50	36.12	38.00	66.80	40.31
BoxInst [91]	40.30	68.70	40.00	28.80	49.10	36.80
Mask2Former [29]	29.60	44.85	29.55	35.03	54.80	34.20
CATNet [5]	51.82	83.40	59.70	55.85	82.53	63.20
HQ-ISNet [1]	53.18	82.92	55.80	56.33	82.03	62.48
SAM-seg (Mask2Former)	40.56	51.04	44.81	45.11	57.54	45.48
SAM-seg (Mask R-CNN)	62.83	87.16	71.21	57.40	82.80	61.70
SAM-cls	38.87	63.64	39.75	37.85	61.62	40.63
SAM-det	63.71	89.23	75.06	59.76	84.54	59.80
RSPrompter-query	58.79	77.53	66.12	65.29	85.77	65.54
RSPrompter-anchor	68.54	90.80	83.25	67.64	87.70	69.37

TABLE III

THE TABLE DISPLAYS A COMPARISON BETWEEN THE PROPOSED METHOD AND OTHER STATE-OF-THE-ART METHODS ON THE SSDD DATASET. IT PRESENTS AP(%) VALUES FOR BOXES AND MASKS AT VARIOUS IOU THRESHOLDS.

Method	AP _{box}	AP _{box} ⁵⁰	AP _{box} ⁷⁵	AP _{mask}	AP _{mask} ⁵⁰	AP _{mask} ⁷⁵
Mask R-CNN [20]	63.40	92.62	77.93	60.92	92.62	75.68
Mask Scoring R-CNN [22]	67.71	96.80	80.59	64.16	95.66	84.27
HTC [23]	67.56	95.02	76.00	63.28	94.76	83.94
InstaBoost [87]	54.77	87.85	58.54	58.95	89.05	71.57
SOLO [28]	53.60	87.26	59.82	55.27	89.75	63.99
PointRend [88]	63.21	99.87	66.45	63.86	99.80	69.93
SOLO v2 [89]	51.40	82.50	57.54	52.42	89.27	60.07
SCNet [90]	67.25	95.74	83.38	62.66	94.75	76.53
CondInst [27]	57.89	92.53	67.40	50.31	90.46	54.80
BoxInst [91]	44.76	83.75	44.11	34.10	71.16	27.27
Mask2Former [29]	53.40	78.45	67.02	56.52	85.10	69.48
CATNet [5]	64.66	96.46	79.81	64.11	96.35	77.87
HQ-ISNet [1]	65.58	95.48	80.76	64.75	95.26	81.70
SAM-seg (Mask2Former)	49.08	73.43	55.20	54.03	79.65	66.53
SAM-seg (Mask R-CNN)	62.41	94.32	75.38	59.46	92.79	72.17
SAM-cls	34.43	75.85	24.82	40.37	86.17	36.87
SAM-det	69.42	98.70	90.04	64.09	98.70	81.32
RSPrompter-query	66.50	95.80	81.81	64.57	95.97	81.67
RSPrompter-anchor	73.09	99.95	91.56	72.61	99.98	93.24

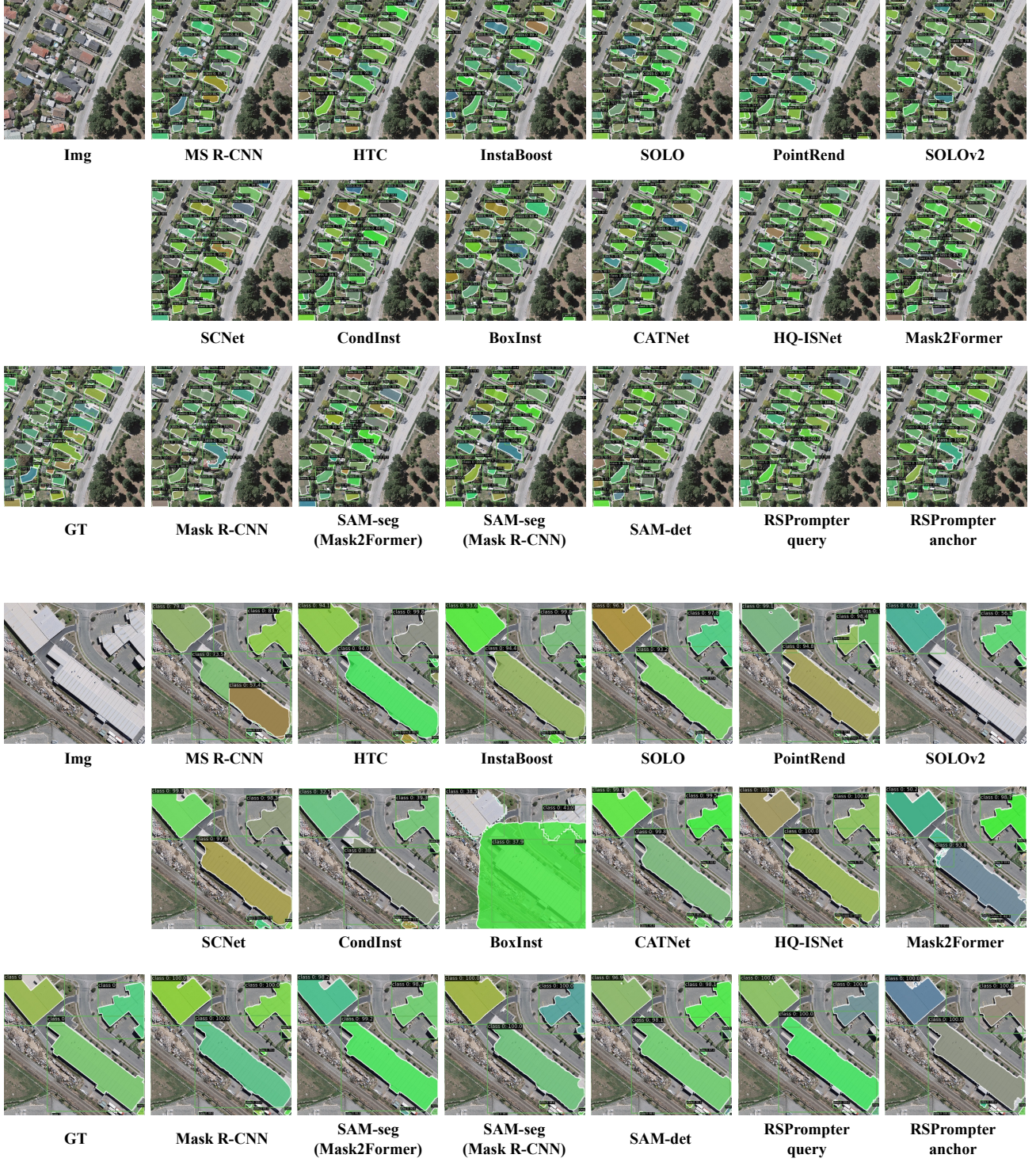


Fig. 7. The visualization showcases segmentation results for several image examples from the WHU dataset, comparing our proposed method with other state-of-the-art methods. Distinct colors indicate different instances.

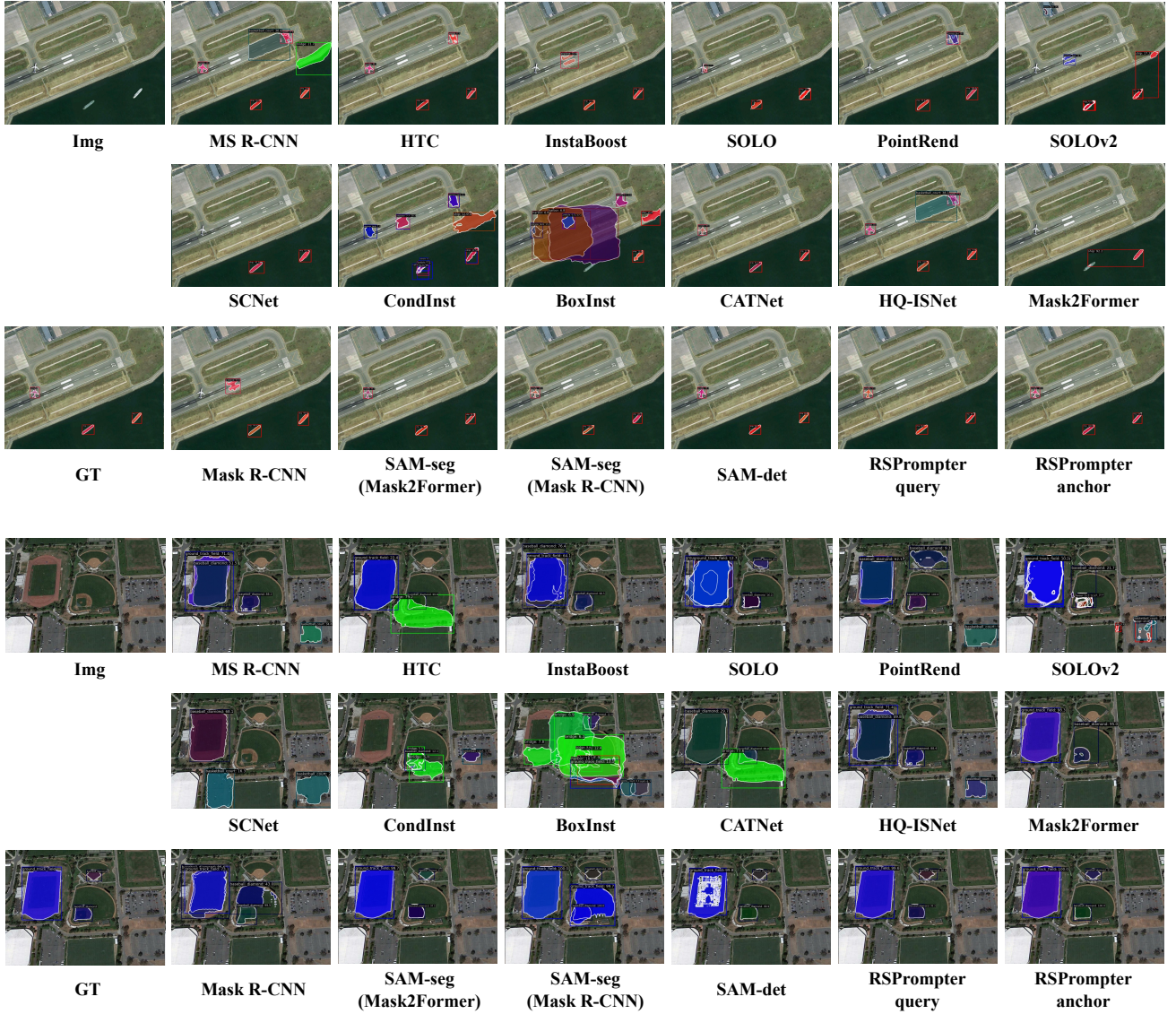


Fig. 8. The visualization highlights segmentation results for a selection of image examples from the NWPU dataset, comparing our proposed method to various other state-of-the-art methods. Each color represents a unique instance.

Mask R-CNN and Mask2Former heads and training regimes. SAM-cls is considered a minimalistic instance segmentation method that leverages the “everything” mode of SAM to obtain all instances in the image and employs a pre-trained ResNet18 [68] to label all instance masks. SAM-det denotes the first training of a Faster R-CNN [39] detector to acquire boxes and subsequently generating corresponding instance masks by SAM with the box prompts. RSPrompter-query and RSPrompter-anchor respectively represent the query-based and anchor-based promoters. All the cited methods are implemented following the official publications using PyTorch.

1) *Quantitative Results on the WHU Dataset:* The results of RSPrompter in comparison to other methods on the WHU dataset are presented in Tab. I, with the best performance highlighted in bold. The task involves performing single-class instance segmentation of buildings in optical RGB band remote sensing images. RSPrompter-query attains the best performance for both box and mask pre-

dictions, achieving AP_{box} and AP_{mask} values of 70.36/69.21. Specifically, SAM-seg (Mask2Former) surpasses the original Mask2Former (60.40/62.77) with 67.84/66.66 on AP_{box} and AP_{mask} , while SAM-seg (Mask R-CNN) exceeds the original Mask R-CNN (56.11/60.75) with 67.15/64.86. Furthermore, both RSPrompter-query and RSPrompter-anchor improve the performance to 70.36/69.21 and 68.06/66.89, respectively, outperforming SAM-det, which carries out detection before segmentation.

These observations suggest that the learning-to-prompt approach effectively adapts SAM for instance segmentation tasks in optical remote sensing images. Moreover, they demonstrate that the SAM backbone, trained on an extensive dataset, can provide valuable instance segmentation guidance even when it is fully frozen (as seen in SAM-seg).

2) *Quantitative Results on NWPU Dataset:* We conduct comparison experiments on the NWPU dataset to further validate RSPrompter’s effectiveness. Unlike the WHU dataset,

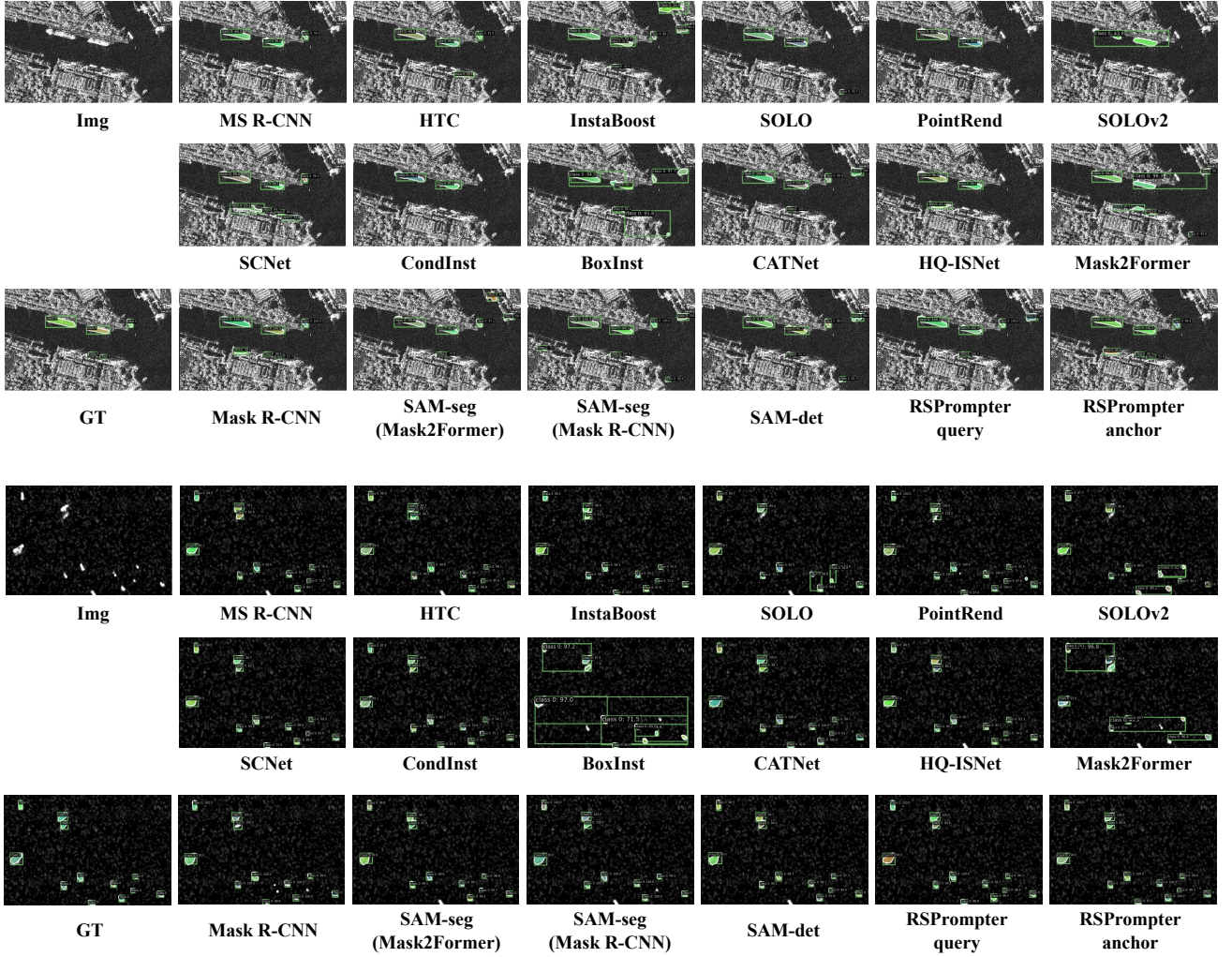


Fig. 9. The visualization demonstrates segmentation results for a number of image examples from the SSDD dataset, comparing our proposed method with several other state-of-the-art methods. Individual colors correspond to different instances.

this one is smaller in size but encompasses more instance categories, amounting to 10 classes of remote sensing objects. The experiment remains focused on optical RGB band remote sensing image instance segmentation. Tab. II exhibits the overall results of various methods on this dataset.

It can be observed that RSPrompter-anchor, when compared to other approaches, generates the best results on box and mask predictions (68.54/67.64). In comparison to Mask R-CNN-based methods, single-stage methods display a substantial decline in performance on this dataset, particularly the Transformer-based Mask2Former. This may be because the dataset is relatively small, making it challenging for single-stage methods to achieve adequate generalization across the full data domain, especially for Transformer-based methods that require a large amount of training data. Nonetheless, it is worth noting that the performance of SAM-based SAM-seg (Mask2Former) and RSPrompter-query remains impressive. The performance improves from 29.60/35.02 for Mask2Former to 40.56/45.11 for SAM-seg (Mask2Former) and further to 58.79/65.29 for RSPrompter-query.

These findings imply that SAM, when trained on a large

amount of data, can exhibit significant generalization ability on a small dataset. Even when there are differences in the image domain, SAM’s performance can be enhanced through the learning-to-prompt approach.

3) *Quantitative Results on SSDD Dataset:* In this study, we carried out an evaluation of the SSDD dataset to thoroughly assess the capability of SAMprompter in performing remote sensing image instance segmentation tasks. The SSDD dataset is a single-category SAR ship instance segmentation dataset, representing a distinctly different modality compared to the previously mentioned datasets and exhibiting significant variations in training data from SAM. Tab. III displays the AP values obtained for different methods on the dataset.

It can be observed that the SAM-seg (Mask2Former) (49.08/54.03) and SAM-seg (Mask R-CNN) (62.41/59.46) approaches, which are based on the SAM backbone, demonstrate lower performance compared to the original Mask2Former (53.40/56.52) and Mask R-CNN (63.40/60.92). This suggests a considerable disparity between the SAM training image domain and the SAR data domain. Nonetheless, SAM-det achieved a significant performance enhance-

ment (69.42/64.09), indicating that employing a detection-first approach followed by SAM for segmentation can yield high performance in SAM’s cross-domain generalization. This is because SAM can provide accurate, category-agnostic, and highly generalized segmentation results with fine-grained intervention prompts. By unlocking the constrained space, RSPrompter-anchor further enhanced the performance to 73.09/72.61, thereby confirming the effectiveness of RSPrompter as well.

4) *Qualitative Visual Comparisons*: To facilitate a more effective visual comparison with other methods, we present a qualitative analysis of the segmentation results obtained from SAM-based techniques and other state-of-the-art instance segmentation approaches. Fig. 7, 8, and 9 depict sample segmentation instances from the WHU dataset, NWPU dataset, and SSDD dataset, respectively. It can be observed that the proposed RSPrompter yields notable visual improvements in instance segmentation. Compared to alternative methods, the RSPrompter generates superior results, exhibiting sharper edges, more distinct contours, enhanced completeness, and a closer resemblance to the ground-truth references.

E. Ablation Study

In this section, we conduct a series of experiments on the NWPU dataset to investigate the importance of each component and parameter setting in our proposed method. Unless otherwise specified, all models are trained using the same configuration with the ViT-Huge image encoder. We restrict our ablation experiments to RSPrompter-query, as its straightforward design led us to regard it as the primary method for this study.

1) Effects of Different Backbone in the Image Encoder:

Different image encoders not only influence the model’s inference speed but also significantly impact its performance. SAM utilizes the MAE pre-trained ViT as its image encoder, which is available in three versions: base, large, and huge. We conducted experiments based on RSPrompter-query using backbones of varying parameter sizes, and Tab. IV illustrates the performance of different backbone versions on the NWPU dataset. As depicted in the table, the instance segmentation performance experiences an upward trend as the backbone network size increases, ranging from 49.45/55.06 to 58.79/65.29 in AP_{box} and AP_{mask} metrics. Depending on the specific application context, different model sizes can be chosen to strike the optimal balance between segmentation efficiency and effectiveness.

2) *Effects of Different Multi-scale Semantic Features in the Aggregator*: The input for the feature aggregator is derived from features at different levels within the ViT backbone. To achieve suitable efficiency, we do not use every layer of the ViT-H as input for the feature aggregator. To demonstrate the impact of varying feature layer selections on the final segmentation outcomes, we conducted experiments presented in Tab. V. The notation [start:end:step] indicates the index of the returned feature map ranging from the start to the end with the specified step size. From the table, it is evident that SAM is not well-suited for extracting class semantic

TABLE IV

THE TABLE BELOW PRESENTS VARIOUS IMAGE ENCODERS, THEIR CORRESPONDING NUMBER OF PARAMETERS, AND THEIR SEGMENTATION PERFORMANCE ON THE NWPU DATASET.

Backbone	Params.	AP_{box}	AP_{box}^{50}	AP_{box}^{75}	AP_{mask}	AP_{mask}^{50}	AP_{mask}^{75}
ViT-B	86M	49.45	66.66	53.09	55.06	70.32	56.02
ViT-L	307M	53.81	69.95	61.41	60.12	78.54	59.90
ViT-H	632M	58.79	77.53	66.12	65.29	85.77	65.54

TABLE V

THE TABLE BELOW HIGHLIGHTS THE IMPACT OF INCORPORATING DIFFERENT HIERARCHICAL FEATURES FROM SAM’S BACKBONE INTO THE FEATURE AGGREGATOR ON SEGMENTATION PERFORMANCE. THE NOTATION [START:END:STEP] SPECIFIES THE INDEX OF THE FEATURE MAPS RETURNED FROM THE START TO THE END WITH A STEP INTERVAL.

Feat.	N Layer	AP_{box}	AP_{box}^{50}	AP_{box}^{75}	AP_{mask}	AP_{mask}^{50}	AP_{mask}^{75}
[0 : 32 : 1]	32	62.24	82.74	73.15	66.25	86.41	69.21
[0 : 32 : 2]	16	61.64	81.62	71.30	66.09	85.95	66.74
[0 : 32 : 4]	8	58.77	76.55	67.08	64.10	82.49	65.69
[0 : 16 : 1]	16	53.64	71.16	58.55	57.82	75.92	58.16
[16 : 32 : 1]	16	57.71	78.07	64.57	62.69	80.50	64.35
[8 : 32 : 1]	24	62.62	82.93	73.57	66.74	86.92	69.55
[8 : 32 : 3]	8	58.79	77.53	66.12	65.29	85.77	65.54

information and generating prompts when using features from either excessively shallow or deep layers. For the sake of prompt generation efficiency, we extracted features every three layers from the 8th layer to the final layer for input into the feature aggregator.

3) *Effects of DownConv and Residual Connection in the Aggregator*: In our pursuit of a lightweight feature aggregator with robust semantic information, we not only reduced the number of layers extracted from the image encoder (from 32 to 8) but also minimized the dimensionality of the extracted feature maps by decreasing the number of channels and spatial dimensions (channels from 1280 to 32, and spatial dimensions from 64×64 to 32×32). Moreover, we introduced residual connections between layers to enhance the flow of semantic information, as illustrated in Fig. 4. The impact of these design elements on the final segmentation results is reported in Tab. VI. As evidenced by the table, reducing the spatial and channel dimensions does not lead to a substantial decline in performance. This indicates that in SAM, providing a fuzzy instance prompt is sufficient to obtain a reasonably accurate mask.

Nevertheless, the absence of residual connections significantly impacts the final segmentation performance, suggesting that a fully serial structure is not appropriate for aggregating features from different layers of ViT. We further proposed a parallel feature aggregation structure that concatenates all extracted feature layers for prompt generation. However, this approach did not yield optimal performance either.

4) *Effects of Different Number of Self-attention and Cross-attention Layers in the Prompter*: The RSPrompter-query incorporates the structure of the Transformer encoder and decoder, based on DETR [42]. The encoder enhances the integration of semantic information from the image backbone’s features, while the decoder interacts with the learnable token embedding and semantic information to obtain the final prompt embedding, as illustrated in Fig. 6. In our method, we exper-

TABLE VI

THE IMPACT OF DOWNCONV AND RESIDUAL CONNECTION IN THE FEATURE AGGREGATOR ON SEGMENTATION PERFORMANCE. THE FIRST ROW DESCRIBES THE APPROACH THAT WAS ULTIMATELY ADOPTED. **RS**: REDUCING THE SPATIAL DIMENSION; **RC**: REDUCING THE CHANNEL DIMENSION; **ARC**: ADDING RESIDUAL CONNECTION; **PC**: PARALLEL ARCHITECTURE WITH FEATURE CONCATENATION.

RS	RC	ARC	PC	AP _{box}	AP _{box} ⁵⁰	AP _{box} ⁷⁵	AP _{mask}	AP _{mask} ⁵⁰	AP _{mask} ⁷⁵
✓	✓	✓		58.79	77.53	66.12	65.29	85.77	65.54
	✓			59.43	76.59	66.31	65.44	83.72	66.49
✓		✓		60.32	78.28	67.29	65.27	84.20	66.03
✓	✓			47.91	63.60	52.34	52.79	68.41	52.67
✓	✓		✓	51.48	67.88	56.60	56.33	71.79	57.01

TABLE VII

THE TABLE BELOW PRESENTS THE IMPACT OF VARYING THE NUMBER OF TRANSFORMER ENCODER AND DECODER LAYERS IN THE PROMPTER ON THE SEGMENTATION PERFORMANCE.

Enc.	Dec.	AP _{box}	AP _{box} ⁵⁰	AP _{box} ⁷⁵	AP _{mask}	AP _{mask} ⁵⁰	AP _{mask} ⁷⁵
1	1	58.39	77.93	65.31	62.19	81.93	62.01
1	2	60.44	79.42	67.40	64.21	83.17	64.78
1	4	58.79	77.53	66.12	65.29	85.77	65.54
1	6	58.34	77.04	65.50	60.68	78.38	60.93
2	4	56.13	71.47	63.06	61.82	78.80	61.20
4	4	54.79	72.89	63.02	56.54	74.21	57.66

mented with various numbers of encoder and decoder layers, as displayed in Tab. VII. The table demonstrates that different numbers of Transformer layers do not significantly impact the final segmentation performance. To ensure efficiency, we chose 1 encoder layer and 4 decoder layers. It is worth noting that the selection of layer numbers is closely related to the dataset size, and larger datasets may benefit from an increased number of layers.

5) *Effects of Query Numbers and Prompt Embedding Numbers in the Prompter*: The prompter can generate N_p sets of prompts for each image, with each set representing an instance mask. Each set contains k_p prompts, where k_p can be considered as the number of points representing a target instance. These two parameters significantly influence the final segmentation results, leading us to conduct controlled experiments on them, as illustrated in Tab. VIII. We tested N_p values of 40, 60, 80, and 100 while setting k_p at 3, 4, 5, and 6. The results indicate that the best performance is achieved when $N_p = 60$ and $k_p = 4$. To analyze the design of these parameters, we examined the distribution of instance numbers within the dataset and found that it resembles the value of N_p . Consequently, we suggest that the choice of N_p should take into account the number of targets per image present in the dataset. The selection of k_p should not be too small or too large: if it is too small, it cannot adequately represent complex instances; if too large, it deviates from the distribution of the original number of SAM prompts. We observed similar trends in the other two datasets as well.

6) *Effects of Applying Sine Regularization for Prompt Embedding Generation in the Prompter*: The original SAM prompt encoder maps a coordinate-based prompt to high-frequency embeddings, which control the decoding of masks through Fourier encoding. However, the feature generated by the prompter is smooth due to the inherent character-

TABLE VIII

THE TABLE BELOW HIGHLIGHTS THE IMPACT OF VARYING QUERY NUMBERS AND PROMPT EMBEDDING NUMBERS IN THE PROMPTER ON SEGMENTATION PERFORMANCE.

N_p	k_p	AP _{box}	AP _{box} ⁵⁰	AP _{box} ⁷⁵	AP _{mask}	AP _{mask} ⁵⁰	AP _{mask} ⁷⁵
40	4	56.96	72.95	62.37	61.49	77.86	60.24
60	4	58.79	77.53	66.12	65.29	85.77	65.54
80	4	57.13	75.81	62.79	62.26	80.15	63.37
100	4	52.30	71.24	56.14	55.54	75.52	54.17
60	3	58.52	76.70	66.91	61.58	78.19	61.40
60	4	58.79	77.53	66.12	65.29	85.77	65.54
60	5	58.26	76.73	63.78	60.71	78.45	60.25
60	6	54.54	76.00	61.59	56.44	77.30	56.98

istics of neural networks. To align the prompt embeddings from both ways, we employ a sine function to directly map the prompter's output into the high-frequency space. The effectiveness of this design is demonstrated in the second row of Tab. IX. The experimental results show that without the sine transformation, the performance metrics drop from 58.79/65.29 to 57.86/63.83 in AP_{box} and AP_{mask}.

7) *Effects of Trainable Mask Decoder and Feature Fusion in the Mask Decoder*: The mask decoder in SAM features a lightweight design, which prompts us to consider incorporating it into the training process. To explore this direction, we conducted experiments, and the results with the mask decoder involved in the training process are shown in the third row of Tab. IX. It reveals that the segmentation performance decreases, indicating that fine-tuning the SAM decoder with a small amount of data may not always be advisable.

Furthermore, during the prompt embeddings generation process, the prompter produces image feature maps (F'_{img}) that contain semantic information, as depicted in Eq. 9. We attempted to facilitate faster network convergence by fusing (adding) F'_{img} with the feature maps obtained through cross-attention between F_{img} and the prompt in the SAM mask decoder (see the last equation of Eq. 1). However, the experimental results demonstrate that this design does not achieve the desired outcome, and it instead results in decreased performance, as shown in the fourth row of Tab. IX. Nonetheless, involving the mask decoder in the training process was found to improve segmentation performance (as shown in the 5th row of Tab. IX).

8) *Effects of Multi-scale Supervision in the Loss Function*: In RSPrompter-query, the multi-layer Transformer decoder generates tokens (F_{query} in Eq. 9) comprising information at different levels, yet during the forward pass, we only utilize the output of the last decoder layer. To enhance supervision during training, we apply the same Φ_{mlp-cl} on the output of each decoder layer to obtain class predictions. We then utilize the accurate class ground truth to guide the training process. The effectiveness of this design can be observed in the last row of Tab. IX, where the performance metrics improved from 63.25 to 65.29 in AP_{mask}.

F. Discussions

In this paper, we propose a prompt-learning method based on SAM to better facilitate remote sensing image processing

TABLE IX

THE TABLE BELOW DEMONSTRATES THE IMPACT OF SINE REGULARIZATION IN THE PROMPTER, INCORPORATING ADDITIONAL TRAINABLE COMPONENTS IN THE MASK DECODER, AND EMPLOYING A MULTI-SCALE TRAINING REGIME ON THE SEGMENTATION PERFORMANCE.

Operation	AP _{box}	AP _{box} ⁵⁰	AP _{box} ⁷⁵	AP _{mask}	AP _{mask} ⁵⁰	AP _{mask} ⁷⁵
Ours (none)	58.79	77.53	66.12	65.29	85.77	65.54
w/o sine	57.86	76.07	65.89	63.83	82.44	66.06
w/ train dec.	51.23	67.97	57.78	52.82	69.86	54.45
w/ fusion dec.	48.27	67.06	50.80	50.69	69.62	51.10
w/ train&fusion dec.	57.32	75.75	63.63	61.89	80.11	62.21
w/o ms loss	58.57	76.72	65.59	63.25	81.08	64.96

with foundation models. Methodologically, this approach is not limited to the SAM model and can be applied to various foundation models. Throughout the experimentation process, we have also identified potential areas for improvement.

As noted by the authors of SAM, the mask decoder of SAM is extremely lightweight (4.1M); however, this does not imply that its computation is equally lightweight. The input token number of the mask decoder transformer is substantial ($> 64 \times 64$), and as a prompt-based interactive segmentation head, a forward calculation is required for each group of prompts. Consequently, when dealing with 100 instance targets in a single image, the forward calculation must be performed 100 times, which is computationally intensive. Researchers might consider redesigning this segmentation head for downstream tasks. Additionally, RSPrompter-query, based on optimal matching, converges more slowly than RSPrompter-anchor due to the lack of relatively clear supervisory information. Nevertheless, its network structure is more straightforward, lightweight, and demonstrates better performance on medium and large-scale datasets compared to RSPrompter-anchor. Researchers could explore ways to optimize its convergence speed. Lastly, the prompt learning method proposed in this paper achieves exceptional generalization performance on small datasets, significantly surpassing other approaches. This suggests that when there is insufficient data to train or fine-tune an appropriate network, prompt engineering design can be considered for foundation models.

V. CONCLUSION

In this paper, we introduce RSPrompter, a prompt learning method for remote sensing image instance segmentation that leverages the SAM foundation model. RSPrompter aims to learn how to generate prompt inputs for SAM, allowing it to automatically obtain semantic instance-level masks. In contrast, the original SAM requires additional manually-crafted prompts to achieve category-agnostic masks. RSPrompter's design philosophy is not limited to the SAM model and can be applied to other fundamental models as well. Based on this philosophy, we have devised two specific implementation schemes: RSPrompter-anchor, which is based on pre-set anchors, and RSPrompter-query, which relies on queries and optimal transport matching. Each structure possesses its unique advantages. Additionally, we have surveyed and proposed various methods and variants within the SAM community for this task and compared them to our prompt learning approach. The effectiveness of each component in RSPrompter has been

validated through ablation studies. Concurrently, experimental results on three public remote sensing datasets demonstrate that our method outperforms other state-of-the-art instance segmentation techniques, as well as some additional SAM-based methods.

REFERENCES

- [1] H. Su, S. Wei, S. Liu, J. Liang, C. Wang, J. Shi, and X. Zhang, "Hq-isnet: High-quality instance segmentation for remote sensing imagery," *Remote Sensing*, vol. 12, no. 6, p. 989, 2020.
- [2] H. Su, S. Wei, M. Yan, C. Wang, J. Shi, and X. Zhang, "Object detection and instance segmentation in remote sensing imagery based on precise mask r-cnn," in *IGARSS 2019-2019 IEEE International Geoscience and Remote Sensing Symposium*. IEEE, 2019, pp. 1454–1457.
- [3] T. Zhang, X. Zhang, P. Zhu, X. Tang, C. Li, L. Jiao, and H. Zhou, "Semantic attention and scale complementary network for instance segmentation in remote sensing images," *IEEE Transactions on Cybernetics*, vol. 52, no. 10, pp. 10 999–11 013, 2021.
- [4] X. Xu, Z. Feng, C. Cao, M. Li, J. Wu, Z. Wu, Y. Shang, and S. Ye, "An improved swin transformer-based model for remote sensing object detection and instance segmentation," *Remote Sensing*, vol. 13, no. 23, p. 4779, 2021.
- [5] Y. Liu, H. Li, C. Hu, S. Luo, H. Shen, and C. W. Chen, "Catnet: context aggregation network for instance segmentation in remote sensing images," *arXiv preprint arXiv:2111.11057*, 2021.
- [6] Z. Zou, K. Chen, Z. Shi, Y. Guo, and J. Ye, "Object detection in 20 years: A survey," *Proceedings of the IEEE*, 2023.
- [7] K. Chen, Z. Zou, and Z. Shi, "Building extraction from remote sensing images with sparse token transformers," *Remote Sensing*, vol. 13, no. 21, p. 4441, 2021.
- [8] K. Chen, W. Li, J. Chen, Z. Zou, and Z. Shi, "Resolution-agnostic remote sensing scene classification with implicit neural representations," *IEEE Geoscience and Remote Sensing Letters*, 2022.
- [9] J. Chen, K. Chen, H. Chen, Z. Zou, and Z. Shi, "A degraded reconstruction enhancement-based method for tiny ship detection in remote sensing images with a new large-scale dataset," *IEEE Transactions on Geoscience and Remote Sensing*, vol. 60, pp. 1–14, 2022.
- [10] G. Cheng and J. Han, "A survey on object detection in optical remote sensing images," *ISPRS journal of photogrammetry and remote sensing*, vol. 117, pp. 11–28, 2016.
- [11] W. Li, K. Chen, and Z. Shi, "Geographical supervision correction for remote sensing representation learning," *IEEE Transactions on Geoscience and Remote Sensing*, vol. 60, pp. 1–20, 2022.
- [12] K. Li, G. Wan, G. Cheng, L. Meng, and J. Han, "Object detection in optical remote sensing images: A survey and a new benchmark," *ISPRS journal of photogrammetry and remote sensing*, vol. 159, pp. 296–307, 2020.

- [13] H. Chen, H. Zhang, K. Chen, C. Zhou, S. Chen, Z. Zhou, and Z. Shi, "Remote sensing image change detection towards continuous bitemporal resolution differences," *arXiv preprint arXiv:2305.14722*, 2023.
- [14] K. Chen, W. Li, S. Lei, J. Chen, X. Jiang, Z. Zou, and Z. Shi, "Continuous remote sensing image super-resolution based on context interaction in implicit function space," *IEEE Transactions on Geoscience and Remote Sensing*, 2023.
- [15] J. Chen, K. Chen, H. Chen, W. Li, Z. Zou, and Z. Shi, "Contrastive learning for fine-grained ship classification in remote sensing images," *IEEE Transactions on Geoscience and Remote Sensing*, vol. 60, pp. 1–16, 2022.
- [16] S. Liu, L. Qi, H. Qin, J. Shi, and J. Jia, "Path aggregation network for instance segmentation," in *Proceedings of the IEEE conference on computer vision and pattern recognition*, 2018, pp. 8759–8768.
- [17] R. Roscher, M. Volpi, C. Mallet, L. Drees, and J. D. Wegner, "Semcity toulouse: A benchmark for building instance segmentation in satellite images," *ISPRS Annals of the Photogrammetry, Remote Sensing and Spatial Information Sciences*, vol. 5, pp. 109–116, 2020.
- [18] S. Minaee, Y. Boykov, F. Porikli, A. Plaza, N. Kehtarnavaz, and D. Terzopoulos, "Image segmentation using deep learning: A survey," *IEEE transactions on pattern analysis and machine intelligence*, vol. 44, no. 7, pp. 3523–3542, 2021.
- [19] F. Fan, X. Zeng, S. Wei, H. Zhang, D. Tang, J. Shi, and X. Zhang, "Efficient instance segmentation paradigm for interpreting sar and optical images," *Remote Sensing*, vol. 14, no. 3, p. 531, 2022.
- [20] K. He, G. Gkioxari, P. Dollár, and R. Girshick, "Mask r-cnn," in *Proceedings of the IEEE international conference on computer vision*, 2017, pp. 2961–2969.
- [21] Z. Cai and N. Vasconcelos, "Cascade r-cnn: high quality object detection and instance segmentation," *IEEE transactions on pattern analysis and machine intelligence*, vol. 43, no. 5, pp. 1483–1498, 2019.
- [22] Z. Huang, L. Huang, Y. Gong, C. Huang, and X. Wang, "Mask scoring r-cnn," in *Proceedings of the IEEE/CVF conference on computer vision and pattern recognition*, 2019, pp. 6409–6418.
- [23] K. Chen, J. Pang, J. Wang, Y. Xiong, X. Li, S. Sun, W. Feng, Z. Liu, J. Shi, W. Ouyang *et al.*, "Hybrid task cascade for instance segmentation," in *Proceedings of the IEEE/CVF conference on computer vision and pattern recognition*, 2019, pp. 4974–4983.
- [24] D. Bolya, C. Zhou, F. Xiao, and Y. J. Lee, "Yolact: Real-time instance segmentation," in *Proceedings of the IEEE/CVF international conference on computer vision*, 2019, pp. 9157–9166.
- [25] H. Chen, K. Sun, Z. Tian, C. Shen, Y. Huang, and Y. Yan, "Blendmask: Top-down meets bottom-up for instance segmentation," in *Proceedings of the IEEE/CVF conference on computer vision and pattern recognition*, 2020, pp. 8573–8581.
- [26] H. Ying, Z. Huang, S. Liu, T. Shao, and K. Zhou, "Embedmask: Embedding coupling for one-stage instance segmentation," *arXiv preprint arXiv:1912.01954*, 2019.
- [27] Z. Tian, C. Shen, and H. Chen, "Conditional convolutions for instance segmentation," in *Computer Vision–ECCV 2020: 16th European Conference, Glasgow, UK, August 23–28, 2020, Proceedings, Part I 16*. Springer, 2020, pp. 282–298.
- [28] X. Wang, T. Kong, C. Shen, Y. Jiang, and L. Li, "Solo: Segmenting objects by locations," in *Computer Vision–ECCV 2020: 16th European Conference, Glasgow, UK, August 23–28, 2020, Proceedings, Part XVIII 16*. Springer, 2020, pp. 649–665.
- [29] B. Cheng, I. Misra, A. G. Schwing, A. Kirillov, and R. Girdhar, "Masked-attention mask transformer for universal image segmentation," in *Proceedings of the IEEE/CVF Conference on Computer Vision and Pattern Recognition*, 2022, pp. 1290–1299.
- [30] OpenAI, "Gpt-4 technical report," 2023.
- [31] J.-B. Alayrac, J. Donahue, P. Luc, A. Miech, I. Barr, Y. Hasson, K. Lenc, A. Mensch, K. Millican, M. Reynolds *et al.*, "Flamingo: a visual language model for few-shot learning," *Advances in Neural Information Processing Systems*, vol. 35, pp. 23 716–23 736, 2022.
- [32] A. Kirillov, E. Mintun, N. Ravi, H. Mao, C. Rolland, L. Gustafson, T. Xiao, S. Whitehead, A. C. Berg, W.-Y. Lo *et al.*, "Segment anything," *arXiv preprint arXiv:2304.02643*, 2023.
- [33] W. Li, K. Chen, H. Chen, and Z. Shi, "Geographical knowledge-driven representation learning for remote sensing images," *IEEE Transactions on Geoscience and Remote Sensing*, vol. 60, pp. 1–16, 2021.
- [34] J. Ma and B. Wang, "Segment anything in medical images," *arXiv preprint arXiv:2304.12306*, 2023.
- [35] J. Cen, Z. Zhou, J. Fang, W. Shen, L. Xie, X. Zhang, and Q. Tian, "Segment anything in 3d with nerfs," *arXiv preprint arXiv:2304.12308*, 2023.
- [36] R. Zhang, Z. Jiang, Z. Guo, S. Yan, J. Pan, H. Dong, P. Gao, and H. Li, "Personalize segment anything model with one shot," *arXiv preprint arXiv:2305.03048*, 2023.
- [37] L. Ke, M. Ye, M. Danelljan, Y. Liu, Y.-W. Tai, C.-K. Tang, and F. Yu, "Segment anything in high quality," 2023.
- [38] A. M. Hafiz and G. M. Bhat, "A survey on instance segmentation: state of the art," *International journal of multimedia information retrieval*, vol. 9, no. 3, pp. 171–189, 2020.
- [39] S. Ren, K. He, R. Girshick, and J. Sun, "Faster r-cnn: Towards real-time object detection with region proposal networks," *Advances in neural information processing systems*, vol. 28, 2015.
- [40] T.-Y. Lin, P. Dollár, R. Girshick, K. He, B. Hariharan, and S. Belongie, "Feature pyramid networks for object detection," in *Proceedings of the IEEE conference on computer vision and pattern recognition*, 2017, pp. 2117–2125.
- [41] A. Vaswani, N. Shazeer, N. Parmar, J. Uszkoreit, L. Jones, A. N. Gomez, Ł. Kaiser, and I. Polosukhin, "Attention is all you need," *Advances in neural information processing systems*, vol. 30, 2017.

- [42] N. Carion, F. Massa, G. Synnaeve, N. Usunier, A. Kirillov, and S. Zagoruyko, “End-to-end object detection with transformers,” in *Computer Vision—ECCV 2020: 16th European Conference, Glasgow, UK, August 23–28, 2020, Proceedings, Part I 16*. Springer, 2020, pp. 213–229.
- [43] B. Cheng, A. Schwing, and A. Kirillov, “Per-pixel classification is not all you need for semantic segmentation,” *Advances in Neural Information Processing Systems*, vol. 34, pp. 17 864–17 875, 2021.
- [44] M. Minderer, A. Gritsenko, A. Stone, M. Neumann, D. Weissenborn, A. Dosovitskiy, A. Mahendran, A. Arnab, M. Dehghani, Z. Shen *et al.*, “Simple open-vocabulary object detection with vision transformers,” *arXiv preprint arXiv:2205.06230*, 2022.
- [45] F. Liang, B. Wu, X. Dai, K. Li, Y. Zhao, H. Zhang, P. Zhang, P. Vajda, and D. Marculescu, “Open-vocabulary semantic segmentation with mask-adapted clip,” in *Proceedings of the IEEE/CVF Conference on Computer Vision and Pattern Recognition*, 2023, pp. 7061–7070.
- [46] S. Liu, Z. Zeng, T. Ren, F. Li, H. Zhang, J. Yang, C. Li, J. Yang, H. Su, J. Zhu *et al.*, “Grounding dino: Marrying dino with grounded pre-training for open-set object detection,” *arXiv preprint arXiv:2303.05499*, 2023.
- [47] X. Wang, X. Zhang, Y. Cao, W. Wang, C. Shen, and T. Huang, “Seggpt: Segmenting everything in context,” *arXiv preprint arXiv:2304.03284*, 2023.
- [48] X. Zou, J. Yang, H. Zhang, F. Li, L. Li, J. Gao, and Y. J. Lee, “Segment everything everywhere all at once,” *arXiv preprint arXiv:2304.06718*, 2023.
- [49] A. Radford, J. W. Kim, C. Hallacy, A. Ramesh, G. Goh, S. Agarwal, G. Sastry, A. Askell, P. Mishkin, J. Clark *et al.*, “Learning transferable visual models from natural language supervision,” in *International conference on machine learning*. PMLR, 2021, pp. 8748–8763.
- [50] C. Jia, Y. Yang, Y. Xia, Y.-T. Chen, Z. Parekh, H. Pham, Q. Le, Y.-H. Sung, Z. Li, and T. Duerig, “Scaling up visual and vision-language representation learning with noisy text supervision,” in *International Conference on Machine Learning*. PMLR, 2021, pp. 4904–4916.
- [51] J. Devlin, M.-W. Chang, K. Lee, and K. Toutanova, “Bert: Pre-training of deep bidirectional transformers for language understanding,” *arXiv preprint arXiv:1810.04805*, 2018.
- [52] C. Raffel, N. Shazeer, A. Roberts, K. Lee, S. Narang, M. Matena, Y. Zhou, W. Li, and P. J. Liu, “Exploring the limits of transfer learning with a unified text-to-text transformer,” *The Journal of Machine Learning Research*, vol. 21, no. 1, pp. 5485–5551, 2020.
- [53] A. Radford, K. Narasimhan, T. Salimans, I. Sutskever *et al.*, “Improving language understanding by generative pre-training,” 2018.
- [54] A. Radford, J. Wu, R. Child, D. Luan, D. Amodei, I. Sutskever *et al.*, “Language models are unsupervised multitask learners,” *OpenAI blog*, vol. 1, no. 8, p. 9, 2019.
- [55] T. Brown, B. Mann, N. Ryder, M. Subbiah, J. D. Kaplan, P. Dhariwal, A. Neelakantan, P. Shyam, G. Sastry, A. Askell *et al.*, “Language models are few-shot learners,” *Advances in neural information processing systems*, vol. 33, pp. 1877–1901, 2020.
- [56] L. Ouyang, J. Wu, X. Jiang, D. Almeida, C. Wainwright, P. Mishkin, C. Zhang, S. Agarwal, K. Slama, A. Ray *et al.*, “Training language models to follow instructions with human feedback,” *Advances in Neural Information Processing Systems*, vol. 35, pp. 27 730–27 744, 2022.
- [57] X. Zhai, A. Kolesnikov, N. Houlsby, and L. Beyer, “Scaling vision transformers,” in *Proceedings of the IEEE/CVF Conference on Computer Vision and Pattern Recognition*, 2022, pp. 12 104–12 113.
- [58] M. Dehghani, J. Djolonga, B. Mustafa, P. Padlewski, J. Heek, J. Gilmer, A. Steiner, M. Caron, R. Geirhos, I. Alabdulmohsin *et al.*, “Scaling vision transformers to 22 billion parameters,” *arXiv preprint arXiv:2302.05442*, 2023.
- [59] Z. Liu, H. Hu, Y. Lin, Z. Yao, Z. Xie, Y. Wei, J. Ning, Y. Cao, Z. Zhang, L. Dong *et al.*, “Swin transformer v2: Scaling up capacity and resolution,” in *Proceedings of the IEEE/CVF conference on computer vision and pattern recognition*, 2022, pp. 12 009–12 019.
- [60] K. He, X. Chen, S. Xie, Y. Li, P. Dollár, and R. Girshick, “Masked autoencoders are scalable vision learners,” in *Proceedings of the IEEE/CVF Conference on Computer Vision and Pattern Recognition*, 2022, pp. 16 000–16 009.
- [61] K. Chen, X. Jiang, Y. Hu, X. Tang, Y. Gao, J. Chen, and W. Xie, “Ovarnet: Towards open-vocabulary object attribute recognition,” in *Proceedings of the IEEE/CVF Conference on Computer Vision and Pattern Recognition*, 2023, pp. 23 518–23 527.
- [62] C. Feng, Y. Zhong, Z. Jie, X. Chu, H. Ren, X. Wei, W. Xie, and L. Ma, “Promptdet: Towards open-vocabulary detection using uncured images,” in *Computer Vision—ECCV 2022: 17th European Conference, Tel Aviv, Israel, October 23–27, 2022, Proceedings, Part IX*. Springer, 2022, pp. 701–717.
- [63] A. Krizhevsky, I. Sutskever, and G. E. Hinton, “Imagenet classification with deep convolutional neural networks,” *Communications of the ACM*, vol. 60, no. 6, pp. 84–90, 2017.
- [64] M. Z. Alom, T. M. Taha, C. Yakopcic, S. Westberg, P. Sidike, M. S. Nasrin, B. C. Van Esesn, A. A. S. Awwal, and V. K. Asari, “The history began from alexnet: A comprehensive survey on deep learning approaches,” *arXiv preprint arXiv:1803.01164*, 2018.
- [65] O. Russakovsky, J. Deng, H. Su, J. Krause, S. Satheesh, S. Ma, Z. Huang, A. Karpathy, A. Khosla, M. Bernstein *et al.*, “Imagenet large scale visual recognition challenge,” *International journal of computer vision*, vol. 115, pp. 211–252, 2015.
- [66] J. Deng, W. Dong, R. Socher, L.-J. Li, K. Li, and L. Fei-Fei, “Imagenet: A large-scale hierarchical image database,” in *2009 IEEE conference on computer vision and pattern recognition*. Ieee, 2009, pp. 248–255.
- [67] K. Simonyan and A. Zisserman, “Very deep convolutional networks for large-scale image recognition,” *arXiv preprint arXiv:1409.1556*, 2014.

- [68] K. He, X. Zhang, S. Ren, and J. Sun, "Deep residual learning for image recognition," in *Proceedings of the IEEE conference on computer vision and pattern recognition*, 2016, pp. 770–778.
- [69] B. Lester, R. Al-Rfou, and N. Constant, "The power of scale for parameter-efficient prompt tuning," *arXiv preprint arXiv:2104.08691*, 2021.
- [70] M. Jia, L. Tang, B.-C. Chen, C. Cardie, S. Belongie, B. Hariharan, and S.-N. Lim, "Visual prompt tuning," in *Computer Vision–ECCV 2022: 17th European Conference, Tel Aviv, Israel, October 23–27, 2022, Proceedings, Part XXXIII*. Springer, 2022, pp. 709–727.
- [71] P. Liu, W. Yuan, J. Fu, Z. Jiang, H. Hayashi, and G. Neubig, "Pre-train, prompt, and predict: A systematic survey of prompting methods in natural language processing," *ACM Computing Surveys*, vol. 55, no. 9, pp. 1–35, 2023.
- [72] K. Zhou, J. Yang, C. C. Loy, and Z. Liu, "Learning to prompt for vision-language models," *International Journal of Computer Vision*, vol. 130, no. 9, pp. 2337–2348, 2022.
- [73] H. Liu, C. Li, Q. Wu, and Y. J. Lee, "Visual instruction tuning," *arXiv preprint arXiv:2304.08485*, 2023.
- [74] P. Gupta, C. Jiao, Y.-T. Yeh, S. Mehri, M. Eskenazi, and J. P. Bigham, "Improving zero and few-shot generalization in dialogue through instruction tuning," *arXiv preprint arXiv:2205.12673*, 2022.
- [75] B. Peng, C. Li, P. He, M. Galley, and J. Gao, "Instruction tuning with gpt-4," *arXiv preprint arXiv:2304.03277*, 2023.
- [76] J. Wei, X. Wang, D. Schuurmans, M. Bosma, E. Chi, Q. Le, and D. Zhou, "Chain of thought prompting elicits reasoning in large language models," *arXiv preprint arXiv:2201.11903*, 2022.
- [77] X. Wang, J. Wei, D. Schuurmans, Q. Le, E. Chi, and D. Zhou, "Self-consistency improves chain of thought reasoning in language models," *arXiv preprint arXiv:2203.11171*, 2022.
- [78] Z. Zhang, A. Zhang, M. Li, and A. Smola, "Automatic chain of thought prompting in large language models," *arXiv preprint arXiv:2210.03493*, 2022.
- [79] Z. Wang, Z. Zhang, C.-Y. Lee, H. Zhang, R. Sun, X. Ren, G. Su, V. Perot, J. Dy, and T. Pfister, "Learning to prompt for continual learning," in *Proceedings of the IEEE/CVF Conference on Computer Vision and Pattern Recognition*, 2022, pp. 139–149.
- [80] A. Dosovitskiy, L. Beyer, A. Kolesnikov, D. Weissenborn, X. Zhai, T. Unterthiner, M. Dehghani, M. Minderer, G. Heigold, S. Gelly *et al.*, "An image is worth 16x16 words: Transformers for image recognition at scale," *arXiv preprint arXiv:2010.11929*, 2020.
- [81] H. W. Kuhn, "The hungarian method for the assignment problem," *Naval research logistics quarterly*, vol. 2, no. 1-2, pp. 83–97, 1955.
- [82] S. Ji, S. Wei, and M. Lu, "Fully convolutional networks for multisource building extraction from an open aerial and satellite imagery data set," *IEEE Transactions on Geoscience and Remote Sensing*, vol. 57, no. 1, pp. 574–586, 2018.
- [83] G. Cheng, J. Han, P. Zhou, and L. Guo, "Multi-class geospatial object detection and geographic image classification based on collection of part detectors," *ISPRS Journal of Photogrammetry and Remote Sensing*, vol. 98, pp. 119–132, 2014.
- [84] T. Zhang, X. Zhang, J. Li, X. Xu, B. Wang, X. Zhan, Y. Xu, X. Ke, T. Zeng, H. Su *et al.*, "Sar ship detection dataset (ssdd): Official release and comprehensive data analysis," *Remote Sensing*, vol. 13, no. 18, p. 3690, 2021.
- [85] T. Wu, Y. Hu, L. Peng, and R. Chen, "Improved anchor-free instance segmentation for building extraction from high-resolution remote sensing images," *Remote Sensing*, vol. 12, no. 18, p. 2910, 2020.
- [86] T.-Y. Lin, M. Maire, S. Belongie, J. Hays, P. Perona, D. Ramanan, P. Dollár, and C. L. Zitnick, "Microsoft coco: Common objects in context," in *Computer Vision–ECCV 2014: 13th European Conference, Zurich, Switzerland, September 6-12, 2014, Proceedings, Part V 13*. Springer, 2014, pp. 740–755.
- [87] H.-S. Fang, J. Sun, R. Wang, M. Gou, Y.-L. Li, and C. Lu, "Instaboost: Boosting instance segmentation via probability map guided copy-pasting," in *Proceedings of the IEEE/CVF International Conference on Computer Vision*, 2019, pp. 682–691.
- [88] A. Kirillov, Y. Wu, K. He, and R. Girshick, "Pointrend: Image segmentation as rendering," in *Proceedings of the IEEE/CVF conference on computer vision and pattern recognition*, 2020, pp. 9799–9808.
- [89] X. Wang, R. Zhang, T. Kong, L. Li, and C. Shen, "Solov2: Dynamic and fast instance segmentation," *Advances in Neural information processing systems*, vol. 33, pp. 17 721–17 732, 2020.
- [90] T. Vu, H. Kang, and C. D. Yoo, "Scnet: Training inference sample consistency for instance segmentation," in *Proceedings of the AAAI Conference on Artificial Intelligence*, vol. 35, no. 3, 2021, pp. 2701–2709.
- [91] Z. Tian, C. Shen, X. Wang, and H. Chen, "Boxinst: High-performance instance segmentation with box annotations," in *Proceedings of the IEEE/CVF Conference on Computer Vision and Pattern Recognition*, 2021, pp. 5443–5452.
- [92] I. Loshchilov and F. Hutter, "Sgdr: Stochastic gradient descent with warm restarts," *arXiv preprint arXiv:1608.03983*, 2016.